JVI Journals.ASM.org

Molecular Genetic and Biochemical Characterization of the Vaccinia Virus I3 Protein, the Replicative Single-Stranded DNA Binding Protein

Matthew D. Greseth, Kathleen A. Boyle, Matthew S. Bluma, Bethany Unger, Matthew S. Wiebe, Jamaria A. Soares-Martins, Nadi T. Wickramasekera, James Wahlberg, and Paula Traktman

Department of Microbiology and Molecular Genetics, Medical College of Wisconsin, Milwaukee, Wisconsin, USA

Vaccinia virus, the prototypic poxvirus, efficiently and faithfully replicates its ~200-kb DNA genome within the cytoplasm of infected cells. This intracellular localization dictates that vaccinia virus encodes most, if not all, of its own DNA replication machinery. Included in the repertoire of viral replication proteins is the I3 protein, which binds to single-stranded DNA (ssDNA) with great specificity and stability and has been presumed to be the replicative ssDNA binding protein (SSB). We substantiate here that I3 colocalizes with bromodeoxyuridine (BrdU)-labeled nascent viral genomes and that these genomes accumulate in cytoplasmic factories that are delimited by membranes derived from the endoplasmic reticulum. Moreover, we report on a structure/function analysis of I3 involving the isolation and characterization of 10 clustered charge-to-alanine mutants. These mutants were analyzed for their biochemical properties (self-interaction and DNA binding) and biological competence. Three of the mutant proteins, encoded by the I3 alleles I3-4, -5, and -7, were deficient in self-interaction and unable to support virus viability, strongly suggesting that the multimerization of I3 is biologically significant. Mutant I3-5 was also deficient in DNA binding. Additionally, we demonstrate that small interfering RNA (siRNA)-mediated depletion of I3 causes a significant decrease in the accumulation of progeny genomes and that this reduction diminishes the yield of infectious virus.

Vaccinia virus, the prototypic poxvirus, is a large DNA virus that replicates exclusively in the cytoplasm. This lack of access to the DNA replication machinery of the host necessitates that poxviruses encode the proteins required for faithful and efficient replication and maturation of their genome (2, 34). A combination of biochemical, genetic, and genomic approaches has led to the identification of the viral DNA polymerase (E9), a heterodimeric processivity factor (A20 and D4, which is also a uracil DNA glycosylase [UDG]), the D5 protein (the putative primase/helicase), and the I3 single-stranded DNA (ssDNA) binding protein (SSB) as key proteins that function at the replication fork (3, 10–12, 14, 21, 25, 33, 40, 42, 47, 53). Additional proteins also support DNA replication (H5), and yet others are involved in precursor metabolism (J2 and F4/I4), recombination/repair (G5), maturation (A22), and encapsidation (I6 and A32) of the genome (5, 7, 15, 16, 45). Finally, the B1 protein kinase is required to overcome the antiviral effects of the host DNA binding protein BAF. BAF binds to and sequesters the viral DNA, preventing its replication, unless it is phosphorylated on its N′ terminus by B1 (58).

The mode of poxvirus genome replication remains poorly understood. The genome is an ~200-kb linear double-stranded DNA (dsDNA) duplex with covalently closed hairpin termini. The working model of replication (2, 34) posits that replication is initiated by the introduction of a nick near one of the termini, which then provides a primer terminus that can be elongated by the processive viral polymerase. Replication of the terminal loop could position the polymerase to copy both strands of the genome in a leading strand-only mode of replication. Such a replication model would lead to tail-to-tail dimers and higher-order concatemers, which have indeed been seen *in vivo* (2, 35). However, the recent observation that the D5 protein has primase activity *in vitro* (9) suggests that replication might include lagging-strand synthesis, which has not yet been confirmed or excluded. Recombinational priming, which has been seen with some bacteriophages, may also occur.

Regardless of whether or not replication involves leading-strand synthesis only, protection of regions of single-stranded DNA that are exposed during replication would require a replicative SSB. Some years ago, we proposed that the vaccinia virus I3 protein served as the replicative SSB (42). I3 is an abundant 30-kDa protein (with an electrophoretic mobility of ~34 kDa) that is expressed at both early and intermediate times postinfection and binds tightly and specifically to single-stranded DNA. Subsequent reports confirmed the DNA binding properties of I3 and suggested that it facilitates both DNA replication and recombination *in vivo* (14, 53). However, definitive evidence that I3 is the replicative SSB has not yet been presented, nor has a structure/function analysis. The data described in this report address these questions. We describe the generation and analysis of 10 clustered charge-to-alanine mutants of I3 and address the ability of the mutant I3 proteins to bind to DNA and to multimerize *in vitro*. The proteins encoded by three of the alleles generated exhibited defects in one or both of these assays. In addition, we describe the generation of viruses in which the endogenous wild-type (WT) I3 gene has been replaced by these mutant alleles and report that the same three mutant alleles of the I3 gene are unable to support virus viability *in*

Received 25 January 2012 **Accepted** 9 March 2012
Published ahead of print 21 March 2012
Address correspondence to Paula Traktman, ptrakt@mcw.edu.
M.D.G. and K.A.B. contributed equally to this article.
Supplemental material for this article may be found at http://jvi.asm.org/.
Copyright © 2012, American Society for Microbiology. All Rights Reserved.
doi:10.1128/JVI.00206-12

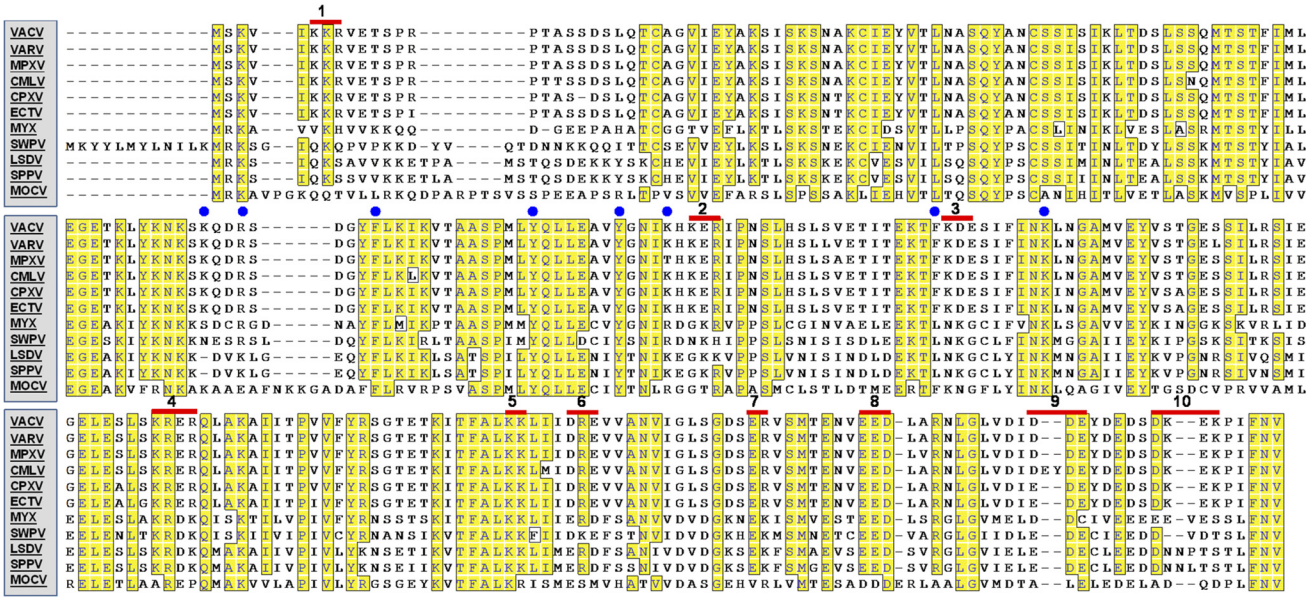

FIG 1 Alignment of poxviral I3 homologs and identification of residues targeted for mutagenesis. An alignment of the predicted primary amino acid sequence of the I3 proteins encoded by vaccinia (VACV), variola (VARV), monkeypox (MPXV), camelpox (CMLV), cowpox (CPXV), ectromelia (ECTV), myxoma (MYX), swinepox (SWPV), lumpy skin disease (LSDV), sheeppox (SPPV), and molluscum contagiosum (MOCV) viruses (the sequences were obtained from www.poxvirus.org). Shaded boxes depict residues that are identical between the vaccinia I3 protein and at least eight other I3 homologs. The blue circles highlight aromatic and basic residues that we hypothesize to correspond to a conserved DNA binding signature conserved in many SSBs; red lines depict clustered charge-to-alanine mutants generated.

vivo. Finally, we show that small interfering RNA (siRNA)-mediated depletion of I3 leads to a reduction in the accumulation of progeny genomes and viral yield. Cumulatively, these data support the conclusion that I3 is a replicative SSB and shed light on the biochemical properties of the protein.

MATERIALS AND METHODS

Reagents. Restriction endonucleases, T4 DNA ligase, T4 polynucleotide kinase (PNK), calf intestinal phosphatase (CIP), pancreatic RNase, PCR-grade deoxynucleoside triphosphates (dNTPs), *Taq* DNA polymerase, and DNA molecular weight standards were purchased from Roche Diagnostics (Indianapolis, IN) and were used per the manufacturer's specifications. [^{35}S]methionine and [γ-^{32}P]ATP were purchased from Perkin Elmer Life Sciences (Boston, MA). A peptide carrying three copies of a FLAG tag (3×FLAG-peptide) and EZview Red anti-FLAG M2 Affinity gel beads were obtained from Sigma (St. Louis, MO). Lipofectamine 2000, Geneticin (G418 sulfate) and ^{14}C-labeled protein molecular weight markers were purchased from Invitrogen (Carlsbad, CA). A T7 Coupled Reticulocyte Lysate System for *in vitro* coupled transcription/translation (IVTT) was purchased from Promega (Madison, WI). siRNA duplexes were purchased from Dharmacon RNAi Technologies (Lafayette, CO). Oligonucleotide primers were purchased from Integrated DNA Technologies (IDT; Coralville, IA). Protran nitrocellulose was obtained from Whatman, Inc. (Dassel, Germany).

Cells and virus. Monolayer cultures of African green monkey BSC40 cells were maintained at 37°C in Dulbecco modified eagle medium (DMEM; Invitrogen) containing 5% fetal calf serum (FCS). Viral stocks were prepared from cytoplasmic lysates of infected BSC40 cells by ultracentrifugation through 36% sucrose; titers were determined by plaque assays performed on BSC40 cells. For virological studies, 31.5°C and 39.7°C were used as the permissive and nonpermissive temperatures, respectively.

Targeted mutagenesis and cloning of the I3 gene. Ten regions within the I3 open reading frame (ORF) were chosen for clustered charge-to-alanine mutagenesis (Fig. 1) (8, 16, 40). An overlap PCR strategy was used to introduce the targeted mutations using the cloned HindIII I fragment as a template and the primers listed in Table S1 in the supplemental material. Two sequential rounds of PCR were performed to generate products that overlapped by 17 bp. In the first round, two separate reactions using primers U(x) plus X_B and primers X_C and D(x) were performed. One microliter of each of the two reaction products was mixed and served as the template for a third PCR, which was performed using the U(x) and D(x) primers. The final PCR product was glass purified and digested with BamHI. The pUC-Neo vector (29) was digested with BamHI, treated with CIP, and ligated to the similarly digested insert. The pUC-Neo vector contains the neomycin resistance (Neo) gene under the regulation of the vaccinia virus p7.5 constitutive promoter. All constructs were subjected to DNA sequencing to confirm the presence of the desired mutation and the absence of spurious mutations. The WT allele and all 10 clustered charge-to-alanine alleles of the I3 gene were also amplified using the Cloning U and Cloning D primers; following digestion with NdeI and BamHI, the inserts were ligated into pTM1-3×FLAG and pET14b vectors that had been similarly digested and treated with CIP. The resultant plasmids encode 3×FLAG- and His_6-tagged versions of each I3 allele.

Transient dominant selection and isolation of I3 mutants. Transient dominant selection was used to replace the endogenous I3 ORF with the mutant alleles (8, 13, 16, 26, 29, 40). All infections were performed at 31.5°C to ensure that temperature-sensitive (*ts*) viruses could be isolated. BSC40 cells in 35-mm dishes were infected with WT virus (multiplicity of infection [MOI] of 0.03). At 3 h postinfection (hpi), 3.5 μg of supercoiled pUC/Neo-I3 DNA was introduced into cells using Lipofectamine 2000 (Invitrogen) per the manufacturer's recommendations, and cells were placed at 31.5°C. At 16 hpi, Geneticin (G418 sulfate) was added to a final concentration of 3 mg per ml to select for viral recombinants. Transfections were harvested at 48 hpi, and Neo^r viruses were isolated by two rounds of plaque purification in the presence of G418. Integration of the Neo cassette was confirmed by PCR analysis. Further plaque purification was performed in the absence of drug selection to enable recombinational resolution of the tandem repeats and subsequent loss of the Neo gene. To identify the plaques that lost Neo and retained the mutant I3 allele, rather

than the WT I3 allele, either DNA sequencing or allele-specific PCR was performed. Plaques of the appropriate genomic structure were subjected to sequential rounds of plaque purification until all (≥20) progeny plaques lacked Neo and contained only the mutant I3 allele. These plaques were expanded, and viral stocks were prepared. For mutants 4, 5 and 7, we observed that all plaques that had undergone recombinational resolution and had lost Neo (>20 of which were isolated from each of two independent Neo-positive intermediate viruses) retained the WT I3 allele, whereas none retained the mutant I3 allele. Therefore, we concluded that these three mutant alleles of I3 were unable to support virus viability.

Determination of 24-h viral yield. BSC40 cells in 35-mm dishes were infected at an MOI of 2 and maintained at 31.5°C or 39.7°C. Cells were harvested at 24 hpi, collected by centrifugation, and resuspended in 1 mM Tris (pH 9.0). The cells were disrupted by three cycles of freeze-thawing and two 15-s bursts of sonication. Viral yields were assessed in plaque assays performed on BSC40 cells at 31.5°C. Several independent experiments were performed; for each experiment, viral yield was titrated in duplicate, and the data were averaged and plotted with the standard deviations shown (see Fig. 5B).

***In vitro* transcription/translation of 3×FLAG-I3 and His_6-I3.** The TnT system from Promega was employed for *in vitro* transcription and translation (IVTT) reactions. Fifty-microliter reaction mixtures were programmed according to the manufacturer's instructions using either 750 ng of one of the pET14b-His_6-I3 plasmids or 250 ng of one of the pTM1-3×FLAG-I3 plasmids. The reaction mixtures were incubated for 90 min at 30°C in the presence of 20 μCi of [^{35}S]methionine. One-tenth of each reaction mixture was saved for analysis as input, and the remainder was mixed with other reaction mixtures as appropriate and incubated at room temperature for 1 h with gentle mixing.

The 3×FLAG-I3 and any associated His_6-I3 proteins were retrieved using EZview Red anti-FLAG M2 affinity gel beads. The M2 affinity gel beads were added to the reaction mixtures, along with 300 μl of FLAG lysis buffer (50 mM Tris [pH 7.4], 150 mM NaCl, 1% Triton X-100, 1 mM EDTA, 1 μg/ml leupeptin, 1 μg/ml pepstatin, and 1 mM phenylmethylsulfonyl fluoride [PMSF]), and the samples were incubated with end-over-end rotation for 3 h at 4°C. Beads were retrieved by centrifugation for 30 s at 10,400 × *g*. The beads were washed twice in FLAG-TBS (50 mM Tris [pH 7.4], 150 mM NaCl), and bound proteins were eluted by the addition of FLAG-TBS containing 15 μg of 3×FLAG-peptide (Sigma-Aldrich, St. Louis, MO) for 30 min on ice with gentle agitation. The beads were collected via sedimentation, and the eluate was collected for analysis. Radiolabeled proteins were resolved by SDS-PAGE and visualized by autoradiography. Quantitation was performed using a PhosphorImager Storm Scanner and ImageQuant software.

Induction and purification of recombinant His_6-I3. pET14b-His_6-I3 constructs were transformed into the HMS174 strain of *Escherichia coli*. Cultures were grown in the presence of 0.2% maltose, and I3 expression was induced by infection with bacteriophage λCE6 (MOI of 10), which encodes T7 RNA polymerase. Induction was performed for 3 h (30 min at 37°C and 2.5 h at room temperature), after which bacteria were collected by sedimentation and lysed in 10 ml of pET lysis buffer (20 mM Tris [pH 8.0], 500 mM NaCl, 20 mM imidazole, 0.1% Triton X-100, 10% glycerol, 5 mg/ml lysozyme, 1 μg/ml leupeptin, 1 μg/ml pepstatin, and 1 mM PMSF) and incubated on ice for 30 min. Lysates were sonicated twice for 15 s and clarified by centrifugation at 17,211 × *g* for 30 min. Recombinant His_6-I3 protein was purified by affinity chromatography using a HisTrap FF column and an AKTA fast protein liquid chromatography (FPLC) system (GE Healthcare Life Sciences, Piscataway, NJ). The column was washed and developed with buffer (20 mM Tris [pH 8.0], 500 mM NaCl, 20 mM imidazole, 0.1% Triton X-100, 10% glycerol, 1 μg/ml leupeptin, 1 μg/ml pepstatin, and 1 mM PMSF) containing increasing concentrations of imidazole. The peak of His_6-I3 eluted at 250 mM imidazole; pooled fractions were dialyzed against a buffer containing 50 mM Tris (pH 7.4), 250 mM NaCl, 1 mM EDTA, 10 mM β-mercaptoethanol, and 25% glycerol and stored at −80°C. Purifications were performed from 100- to 500-ml cultures.

Electromobility shift assays (EMSAs). The 24-mer oligonucleotide probe (5′-CGTGTCGCCCTTATTCCGATAGTG-3′) was radiolabeled at its 5′ terminus with [γ-^{32}P]ATP and T4 polynucleotide kinase. Thirty or ninety nanograms of each I3 preparation was incubated with 2.4 pmol of radiolabeled probe for 15 min at 30°C in a 15-μl reaction mixture containing 250 μg of bovine serum albumin (BSA) per ml, 20 mM Tris (pH 7.4), 50 mM NaCl, 1 mM EDTA, and 5% glycerol. The samples were then resolved electrophoretically on 15-cm vertical, nondenaturing 10% polyacrylamide gels which were cast and run in 0.25× Tris borate-EDTA (TBE) (final concentrations of 22.25 mM Tris, 22.25 mM boric acid, 0.5 mM EDTA); electrophoresis was performed at 200 V for 4 h at 4°C. Gels were dried and exposed for autoradiography. Bands were quantified using a PhosphorImager Storm Scanner and ImageQuant software.

Gel filtration analysis of recombinant I3. A total of 250 μg of purified recombinant His_6-I3 protein and 100 μg each of individual gel filtration standards (Bio-Rad, Hercules, CA) (thyroglobulin [670,000 Da], gamma globulin [158,000 Da], ovalbumin [44,000 Da], and myoglobin [17,000 Da]) were mixed together and adjusted to contain 50 mM Tris (pH 7.4), 150 mM NaCl, 1 mM EDTA, 10 mM β-mercaptoethanol, and 10% glycerol. The sample was injected onto a HiPrep 16/60 Sephacryl S-100 High Resolution column (GE Healthcare Life Sciences) that was equilibrated and then developed in the same buffer. Chromatography was performed at 0.45 ml/min on an AKTA FPLC apparatus at 10°C. One-milliliter fractions were collected, and the elution profile of I3 was determined by SDS-PAGE, followed by silver stain and immunoblot analysis.

siRNA-mediated interference. Twenty-one-nucleotide (nt) RNA duplexes (each strand possessing a terminal 3′ dT dinucleotide) were purchased from Dharmacon RNAi Technologies. siRNA sequences can be found in Table S1 in the supplemental material. Each siRNA duplex (20 nM) was transfected into BSC40 cells that had been seeded the day prior at a density of 2.25 × 10^5 cells/35-mm dish, using *Trans*IT-TKO transfection reagent (Mirus Bio LLC, Madison, WI) as directed per manufacturer specifications. At 18 h posttransfection, cells were infected with WT virus (MOI of 3) and harvested at the time points indicated (see Fig. 6).

Immunoblot analysis of viral proteins. Whole-cell extracts were prepared from siRNA-treated, virally infected cells, resolved on SDS–15% acrylamide gels, and transferred electrophoretically to nitrocellulose filters. The blots were analyzed by incubation with polyclonal serum directed against A20, I3, or F18 (29, 40, 42), followed by a horseradish peroxidase-conjugated secondary antiserum (Bio-Rad). After development with chemiluminescent Super Signal WestPico reagents (Pierce, Rockford, IL), immunoreactive proteins were visualized on Kodak MR film or captured by exposure on a FluorChem HD2 documentation system (ProteinSimple, Santa Clara, CA) and quantified using AlphaView software (ProteinSimple).

Southern dot blot hybridization to assess viral DNA accumulation. Infected and mock- or siRNA-treated cells were harvested at the indicated time points (3, 6, 8, 10, 12, and 18 hpi) and subjected to Southern dot blot analysis as previously described (51). DNA was applied to Zeta Probe nitrocellulose (Bio-Rad) and detected using a radiolabeled probe representing the HindIII E and F fragments of the vaccinia virus genome; the bound probe was visualized by autoradiography and quantified on a PhosphorImager Storm Scanner using ImageQuant software. Each sample was spotted in quadruplicate, and the data were averaged and plotted with standard deviations shown.

Pulsed-field gel electrophoresis (PFGE). BSC40 cells were seeded at 2.25 × 10^5 cells per 35-mm dish 1 day prior to being pretreated with siRNA (an siRNA directed against the I3 mRNA or a variant containing 4-nt substitutions predicted to cause mismatches [si-I3 or MM, respectively]) as described above. After 18 h, cells were infected with WT virus (MOI of 3) and harvested at 8 and 12 hpi. A fraction of the cells was reserved for immunoblot analysis. Cell pellets were embedded in 0.5% low-melting-point agarose and digested for 24 h at 50°C with mild agita-

tion in 500 μl of ESP buffer (1% Sarcosyl, 0.5 M EDTA [pH 9.0], 0.5 mg/ml proteinase K). The plugs were equilibrated in 0.5× TBE buffer prior to insertion into premolded wells of a 1% SeaKem Gold agarose gel cast and run in the same buffer. The DNA was resolved on a CHEF Mapper XA apparatus (Bio-Rad) at 6 V/cm for 13 h at 14°C, using a switching time gradient of 1 to 25 s, a linear ramping factor, and a 120° angle. The DNA was visualized by ethidium bromide staining, and the image was captured and quantified using AlphaView software (ProteinSimple). This program allowed resolution of DNA species ranging from >500 kb to ~5 kb. To resolve fragments from 200 kb to ~200 bp, duplicate samples were resolved on the same type of gel at the same temperature using the following parameters: 6 V/cm for 6 h, a switching time gradient of 0.05 s to 17.0 s, a ramping factor of $a = 2.848$ m, and a 120° angle.

Immunofluorescence microscopy. Infected and mock- or siRNA-treated cells were incubated in the presence of bromodeoxyuridine (BrdU) at a final concentration of 25 μg/ml. At 7 hpi, cells were fixed with 4% paraformaldehyde and permeabilized with 0.1% Triton X-100 for 5 min on ice. Samples were then stained with monoclonal anti-BrdU (5 μg/ml; Developmental Studies Hybridoma Bank, University of Iowa, Iowa City, IA) and polyclonal anti-I3 (1:400) antibodies followed by secondary antibodies conjugated to either Alexa Fluor 594 (goat anti-mouse IgG) or Alexa Fluor 488 (goat anti-rabbit IgG) (Invitrogen). For prepermeabilization experiments, infected cells were placed on ice, briefly treated with 0.1% Triton X-100 (30 s), washed, and then fixed and processed as described above.

Immunoelectron microscopy. BSC40 cells were infected with WT virus (MOI of 5) in the presence of BrdU (25 μg/ml, added after 30 min of adsorption) for 7 h and fixed *in situ* with 4% paraformaldehyde–0.1% glutaraldehyde in phosphate-buffered saline (PBS) for 60 min at room temperature. Cells were processed for immunoelectron microscopy and embedded in Lowicryl K4M; grids were stained using either anti-BrdU, anti-I3, or anti-protein disulfide isomerase ([PDI] monoclonal 1D3, Enzo Life Sciences, Ann Arbor, MI) antibodies, followed by incubation with a secondary antibody conjugated to 10-nm gold particles. Grids were poststained with uranyl acetate and examined on either a Hitachi H-600 or JEOL JEM2100 electron microscope.

Generation of an I3-mCherry fusion construct. To generate the pInt-I3-mCherry construct, the mCherry open reading frame was amplified from the pRSET-mCherry vector (46) using the mCherry 5′ and 3′ primers detailed in Table S1 in the supplemental material. The PCR product was digested with BglII and positioned behind the vaccinia virus G8 promoter in the pInt vector (52) that had been digested with BamHI and treated with CIP. The I3 open reading frame lacking a termination codon (amplified from WT genome; using the Cloning U and I3 no stop 3′ primers) (see Table S1 in the supplemental material) was placed upstream of the mCherry sequence via a unique BamHI site that had been placed immediately upstream of the mCherry coding sequence (mCherry 5′ primer). The sequence of the pInt-I3-mCherry construct was confirmed by restriction enzyme digestion and automated DNA sequencing.

Preparation of digital figures. Original data were scanned on an Epson Perfection scanner (Long Beach, CA) and were adjusted with Adobe Photoshop software (Adobe Systems, Inc., San Jose, CA). Data from EMSAs, and TnTs were acquired on a Storm PhosphorImager (Molecular Dynamics, Sunnyvale, CA) and quantified using ImageQuant software (Molecular Dynamics). Images from immunoblot analysis were acquired using the FluorChem HD2 documentation system (ProteinSimple, Santa Clara, CA). The sequence alignments were performed by using the Clustal W method and Lasergene software (DNASTAR, Inc., Madison, WI) using sequences retrieved from the Poxvirus Bioinformatics Resource Center (http://www.poxvirus.org). Statistical analysis and graph preparation were performed using SigmaPlot software (Systat Software, Chicago, IL). Final figures were assembled and labeled with Canvas software (Deneba Systems, Miami, FL).

RESULTS

The vaccinia virus I3 protein has all of the functional hallmarks of a replicative SSB. It is presumed to play an essential role during infection since attempts to isolate a virus carrying an I3 deletion have been unsuccessful (42). An alignment of the I3 orthologs encoded by closely related (vaccinia, variola, monkeypox, camelpox, cowpox, and ectromelia viruses) and more divergent (myxoma, swinepox, lumpy skin disease, sheeppox, and molluscum contagiosum viruses) chordopoxviruses is shown in Fig. 1. Residues that are shared by the vaccinia I3 protein and at least eight other orthologs are shaded and boxed. Although SSBs from diverse organisms often share a structural feature known as an OB (oligonucleotide/oligosaccharide-binding) fold (36, 49), there is no primary sequence consensus associated with their affinity for single-stranded DNA. A loosely conserved pattern of aromatic and basic residues within the putative DNA binding domain of various SSBs has been identified (55), and candidate residues for such a signature within I3 are shown with blue circles in Fig. 1.

Forward genetic analysis of the I3 protein has been lacking since neither the Condit or Dales collections of temperature-sensitive (*ts*) viruses contain mutants with lesions in the I3 gene (22). With the goal of generating a conditionally lethal mutant, we utilized clustered charge-to-alanine mutagenesis to generate 10 variants of I3 (8, 16–18, 21, 40). The rationale behind this approach is that clusters of charged residues are likely to be exposed on the surface of a given protein, and hence their alteration may compromise protein-protein or protein-DNA interactions without disrupting the overall folding and stability of the target protein. The 10 clusters of charged residues chosen for mutagenesis span the protein sequence and are numbered and marked by red lines in Fig. 1. Some of these clusters are highly conserved in all of the I3 homologs, whereas others are conserved only within the highly related orthopoxviruses. The variant alleles were generated using overlap PCR and then cloned into expression vectors for analysis *in vitro* and *in vivo*.

Clustered charge-to-alanine mutagenesis of the I3 protein: analysis of I3-I3 interaction *in vitro*. We reported some years ago that recombinant I3 was predominantly monomeric in solution. Its elution from a Superdex 75 gel filtration column was indicative of a protein with a Stokes radius of 24.7 Å, which was extrapolated to an apparent molecular weight (MW) of 34,000 (assuming I3 is a globular protein) (42). However, many SSBs function as multimers (27, 39, 41), and since our initial report, an I3-I3 interaction was identified definitively in a global yeast two-hybrid screen of the vaccinia virus proteome (32). The two-hybrid interaction has been verified in our own lab (data not shown); we have also developed an *in vitro* assay to monitor the self-interaction of I3. The WT and mutant alleles of I3 were each inserted into both the pTM1-3×FLAG and pET14b vectors, facilitating T7 RNA-polymerase driven expression of 3×FLAG-I3 and His_6-I3, respectively. These two forms of I3 have distinct electrophoretic mobilities. The proteins were expressed *in vitro* using the TnT coupled transcription/translation system, mixed appropriately, and subjected to affinity purification on anti-FLAG resin. The levels of His_6-I3 which copurified with the cognate 3×FLAG-I3 were visualized by autoradiographic analysis of electrophoretically resolved proteins. The data ($n = 5$) were quantified by phosphorimager analysis after taking into account the individual levels of expression and were normalized to the retrieval obtained with the WT

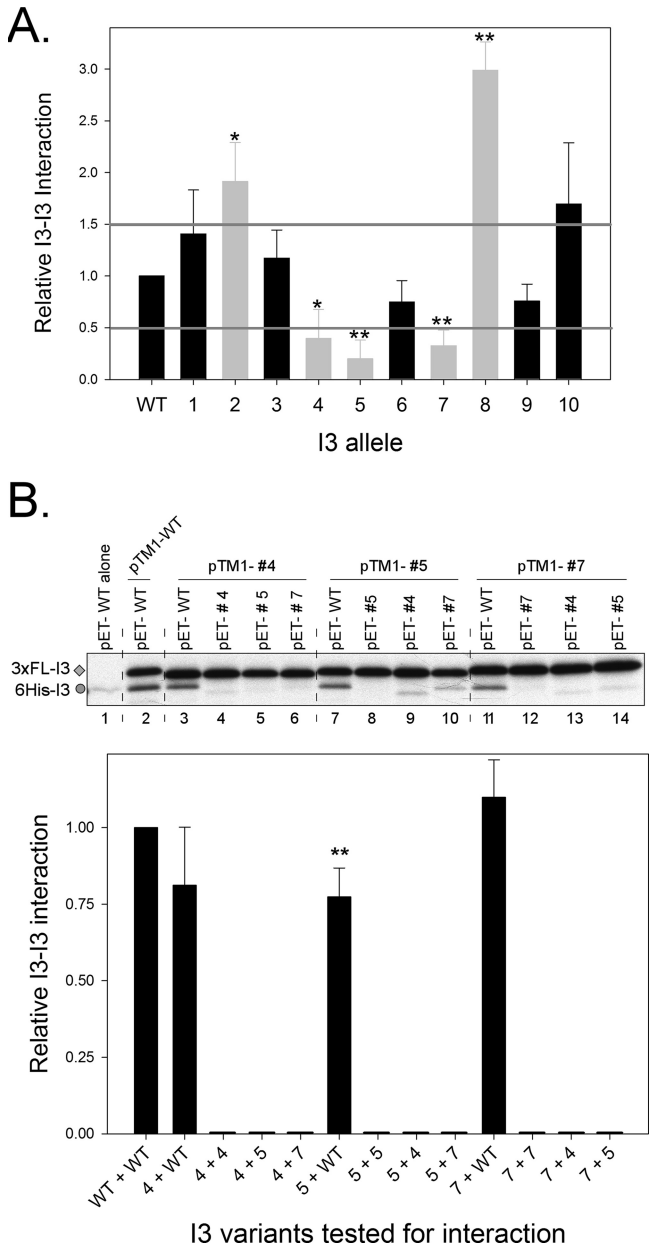

FIG 2 Analysis of I3-I3 self-interaction *in vitro*. Differentially tagged I3 proteins were synthesized in IVTTs, affinity purified, and visualized by autoradiography. (A) Quantification of I3-I3 self-interaction. Values are expressed relative to WT-WT interaction (set to 1) and account for input for each reaction. The gray bars represent statistically significant differences from the WT-WT interaction ($n = 5$; *, $P < 0.05$; **, $P < 0.02$). (B) Additional IVTT reactions were performed characterizing the ability of the defective I3 proteins (shown in panel A) to interact with WT I3 and each other. In the representative autoradiograph shown, the migration of His_6-I3 and 3×FLAG-I3 is represented by the circle and diamond, respectively. Quantification of the I3-I3 self-interactions was performed using the same analysis as described for panel A ($n = 6$; **, $P < 0.02$).

proteins (Fig. 2A). The efficiency of the I3-I3 interaction was within 50% of the value obtained for the WT proteins for most of the mutants. The I3-2 protein showed a modest but significant ($P < 0.05$) increase in self-interaction efficiency above that level, and the I3-8 protein showed a more substantial and significant increase in the efficiency of self-interaction ($P < 0.02$). Most importantly, the I3-4, -5, and -7 proteins showed a statistically significant decrease in (or near ablation of) their ability to self-interact (for I3-4, $P < 0.05$; for I3-5 and -7, $P < 0.02$).

Additional experiments were performed to test the hypothesis that mutants 4, 5, and 7 had a specific defect in self-interaction rather than exhibiting global misfolding (Fig. 2B). First, each of the three mutant proteins was tested for its ability to interact with WT I3 using the same protocol described above. As shown in Fig. 2B, the three His_6-I3 mutant proteins retained the ability to interact with WT 3×FLAG-I3 (Fig. 2B, lanes 3, 7, and 11). For the I3-4 and -7 proteins, the efficiency of this interaction was comparable to the self-interaction of the WT protein (Fig. 2B, lane 2). For the I3-5 protein, a modest but statistically significant diminution in interaction was observed ($P < 0.02$) (Fig. 2B, lane 7). These data argue against a gross misfolding of the I3-4, -5, and -7 proteins. In contrast, these mutant proteins showed little to no ability to interact with themselves or with each other (Fig. 2B, lanes 4 to 6, 8 to 10, and 12 to 14). These data suggest that the three mutations, which map relatively close to each other in the primary sequence of I3, might affect a common binding pocket.

To gain further insight into the multimerization properties of I3, we performed gel filtration analysis of purified preparations of recombinant His_6-I3 protein which were produced in *E. coli* and purified by metal ion affinity chromatography. A total of 250 μg of His_6-WT I3 protein was mixed with protein standards and resolved on a HiPrep 16/60 Sephacryl S100 column. The elution profile showed two distinct peaks of protein (Fig. 3A). The elution profile of the major peak was similar to that of ovalbumin, which has a native molecular weight (MW) of 44,000 (fractions 46 to 49). We interpret this peak as representative of monomeric His_6-I3 (predicted MW of 32,000). An additional peak of protein had an elution profile that overlapped with the thyroglobulin (670 kDa) and immunoglobulin standards (158 kDa), which would be consistent with a higher-order form of I3 that was at least tetrameric (fractions 33 to 36). A similar analysis was performed with purified preparations of mutants 4, 5, and 7. For each of these proteins, only a single peak of I3 was observed: a comparison of fractions 33 to 36 and 46 to 49 from the WT, I3-4, -5, and -7 is shown in Fig. 3B. In each case, I3 was abundant in fractions 46 to 49, but the higher-order species of I3 (fractions 33 to 36) seen for the WT protein was not seen with any of the three mutants. Taken together, the IVTT and gel filtration data strongly suggest that a portion of WT I3 forms multimers in solution, whereas mutants 4, 5, and 7 are deficient in this process.

Clustered charge-to-alanine mutagenesis of the I3 protein: analysis of ssDNA binding *in vitro*. We have previously described the ssDNA binding activity of recombinant (and endogenous) WT I3 using an EMSA (42). We have now extended this analysis to His_6-tagged versions of the WT and mutant I3 proteins. Each affinity-purified recombinant His_6-I3 protein preparation was tested at 30 and 90 ng for its ability to bind a 5′-labeled 24-nt oligonucleotide in an EMSA; a representative autoradiograph (panel A) as well as quantification of replicate experiments ($n = 4$) (panel B) are shown in Fig. 4. Although there was some variability among the DNA binding properties of the different preparations, only two mutants (I3-5 and -6) showed a statistically significant ($P < 0.02$) reduction in DNA binding activity at both protein concentrations. The I3-6 protein was only modestly impaired and exhibited 64 and 56% of the DNA binding activity of the WT

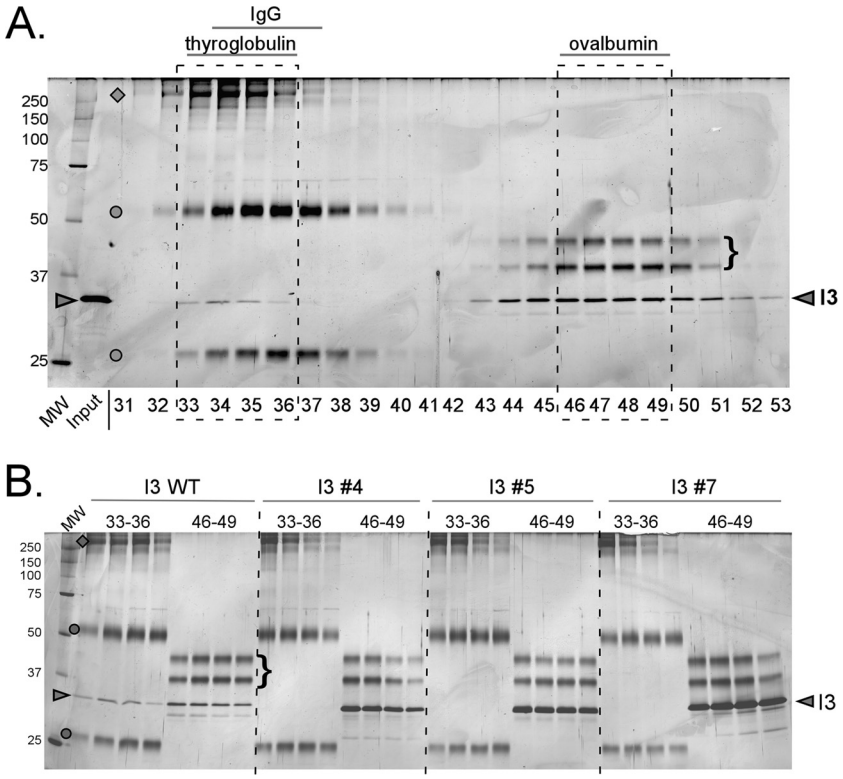

FIG 3 Gel filtration analysis of the multimeric state of I3. (A) A total of 250 μg of purified His_6-WT I3 was combined with 100 μg each of thyroglobulin (670,000 Da), immunoglobulin (158,000 Da), ovalbumin (44,000 Da), and myoglobin (17,000 Da) and resolved on a HiPrep 16/60 Sephacryl S100 high-resolution column. Fractions were collected, and fractions 31 to 53 were resolved by SDS-PAGE and visualized by silver staining. Thyroglobulin, immunoglobulin, ovalbumin, and His_6-WT I3 are represented by diamonds, circles, brackets, and arrowheads, respectively. A total of 250 ng of purified His_6-WT I3 was loaded in the input lane to show the migration of I3. Dashed boxes represent fractions used for further comparative analysis with I3 mutant proteins. (B) Gel filtration analysis was performed on affinity-purified recombinant His_6-I3, -4, -5, and -7 proteins in a similar manner as His_6-WT I3. Identical fractions (33 to 36 and 46 to 49) were subjected to comparative analysis by silver staining. Arrowheads show the position of I3; the MW standards (in thousands) are labeled as described for panel A.

protein at 30 and 90 ng, respectively. The reduction was greater for the I3-5 protein; the DNA binding activity of this protein ranged from 10 to 37% of the WT protein as assayed at 30 and 90 ng, respectively. Thus, the I3-5 protein is diminished both in its capacity to bind DNA and to self-interact. In contrast, the DNA binding activities of mutants 4 and 7 do not appear to be diminished, despite their reduced ability to multimerize. Conversely, mutant 6 shows a modest diminution in DNA-binding activity without any obvious impairment in self-interaction. Cumulatively, these data indicate that the binding of I3 to a 24-mer oligonucleotide *in vitro* does not require oligomerization. Furthermore, it is striking that all of the defects observed in the *in vitro* biochemical assays were found in the proteins encoded by mutant alleles 4 to 7, underscoring the importance of this region of the protein in the function of I3.

Clustered charge-to-alanine mutagenesis of the I3 protein: generation of viral recombinants with altered I3 alleles in an attempt to generate a temperature-sensitive virus. Although the I3 protein is presumed to be the replicative SSB, direct genetic proof of such a role has been lacking. Therefore, the same 10 clustered charge-to-alanine mutants were cloned into an appropriate vector (pUC-Neo) (29) such that transient dominant selection could be used to insert them in place of the endogenous I3 allele within the viral genome. All of the manipulations aimed at isolating these viruses were performed at 31.5°C to ensure the viability of any viruses with temperature-sensitive (*ts*) phenotypes, since *ts* mutants with defects in the vaccinia virus A20, H5, G2, and D1 proteins have been readily obtained using this approach (8, 16–18, 21, 40). Viruses encoding the I3-1, -2, -3, -6, -8, -9, and -10 proteins were readily obtained, extensively plaque purified, and expanded. As shown in Fig. 5A, the plaques formed by these viruses at both 31.5°C and 39.7°C were comparable in size to those formed by WT virus at these temperatures. Likewise, the viral yields obtained after cells were infected for 24 h with each of the viruses at an MOI of 2 were generally equivalent at both temperatures and equivalent to the yield from WT-infected cells (Fig. 5B). A modest decrease in yield was seen at both temperatures for the virus encoding I3-2, but it is unclear whether this difference is of any biological significance. Hence, alleles 1, 2, 3, 6, 8, 9, and 10 were competent to support virus viability in a temperature-insensitive manner. In contrast to these results, we were unable to obtain viruses encoding only the I3-4, -5, or -7 allele despite repeated and concerted efforts. The transient dominant technique involves the isolation of intermediate viruses that, in this case, have tandem duplications of portions of the I2-I3 or I3-I4 region of the genome flanking the Neo gene. This insertion/duplication allows for selection of G418-resistant ($G418^r$) plaques. After the intermediate viruses are isolated, G418 selection is removed, and the duplication is resolved by homologous recombination between the tandem repeats. We had no difficulty isolating these intermediate viruses

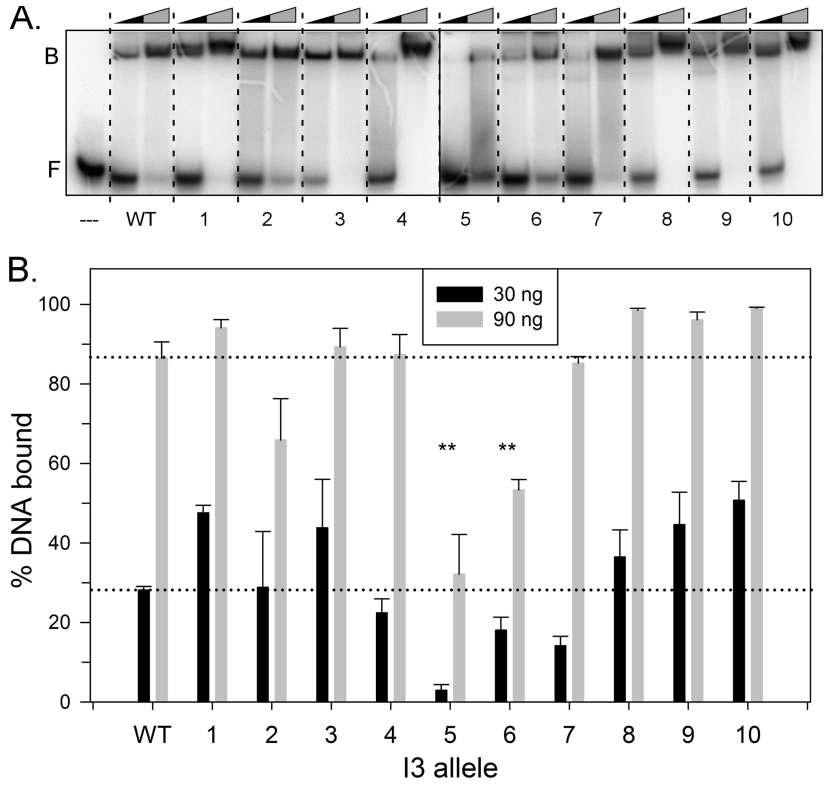

FIG 4 DNA binding analysis of the mutant I3 proteins. (A) EMSAs were performed containing 2.4 pmol of radiolabeled ssDNA oligonucleotide and purified recombinant His_6-I3. Reactions were resolved electrophoretically, and a representative gel is shown. For the WT and I3 mutant preparations, the first and second lanes represent reaction mixtures containing 30 and 90 ng, respectively. The upper band (labeled B) represents ssDNA probe bound to the I3 protein, while the lower band (labeled F) represents the free ssDNA probe. The left-most lane of the blot (—) represent ssDNA probe in the absence of added recombinant protein. (B) Quantification of I3 binding to ssDNA (depicted in panel A). Values are expressed as the ratio of bound probe to bound probe plus free probe: (B/B + F) × 100. Dashed lines represent values obtained for purified WT I3. **, $P < 0.02$.

after transfection of the plasmids encoding the I3-4, -5, or -7 allele, but in each case, all of the resolved viruses retained the WT, and not the mutant, allele. Therefore, we feel confident in concluding that these three mutant alleles are not competent to support virus viability. Interestingly, the three mutants that could not support virus viability are the same three that were defective in self-interaction (Fig. 2); moreover, I3-5 was also defective in DNA binding (Fig. 4). These data suggest that the ability of I3 to form higher-order complexes is likely to play a biologically important role during the infectious cycle.

siRNA-mediated depletion of I3 leads to a diminution in viral DNA replication and 24-h viral yield. Our inability to generate viruses encoding only I3-4, -5, or -7 provided strong evidence that I3 is indeed an essential viral protein. We were not, however, successful in isolating a *ts*I3 virus. As an alternative approach, we generated an siRNA directed against the I3 mRNA (si-I3) as well as a variant containing 4-nt substitutions predicted to cause mismatches and eliminate stable targeting (MM) (sequences can be found in Table S1 in the supplemental material). Our most effective siRNA targeted nucleotides 274 to 292 of the ORF, just downstream of the siRNA previously reported by Gammon and Evans (nt 236 to 256) (14). (An additional oligonucleotide duplex targeting nt 551 to 571 was much less effective in depleting I3 and was not investigated further.) To assess the impact of the siRNA on the steady-state levels of the I3 protein and on viral DNA accumulation on a cell-by-cell basis, cells were infected for 7 h in the presence of BrdU. The incorporation of BrdU into nascent DNA and the levels of I3 were then assessed by immunofluorescence microscopy (42, 51). In mock-treated cells or cells exposed to the MM siRNA (data not shown), we readily observed the presence of large replication foci in which the I3 protein and nascent DNA were colocalized (Fig. 6A, left panels). In cells treated with siRNA directed against I3, the sizes of the I3-positive ($I3^+$) and $BrdU^+$ foci were dramatically and comparably decreased (Fig. 6A, right panels). Hence, the siRNA was effective in depleting I3, which in turn led to a corresponding decrease in DNA synthesis. More quantitative assessments of the depletion of I3 and the levels of DNA synthesis can be obtained from immunoblot and dot blot hybridization analyses, respectively (Fig. 6B and C). The siRNA treatment diminished the levels of I3 to approximately 8 to 10% of those seen in cells treated with MM siRNA (Fig. 6B). This depletion was specific since the levels of other early replication proteins such as UDG (data not shown) and A20 were not impacted. Dot blot hybridization analysis indicated that I3 depletion reduced the accumulation of viral DNA sequences by ~4-fold at the time points studied (Fig. 6C). This reproducible reduction in DNA accumulation is statistically significant ($P < 0.02$ at 6 and 8 hpi; $P < 0.001$ at 10, 12, and 18 hpi) but incomplete, and the accumulation of postreplicative proteins such as F18 (57) is not impaired (Fig. 6B, bottom blot). The 24 h yield of infectious virus under these same conditions was consistently diminished by ~3.3-fold ($P < 0.02$) (Fig. 6D). These data suggest that either I3 is present in

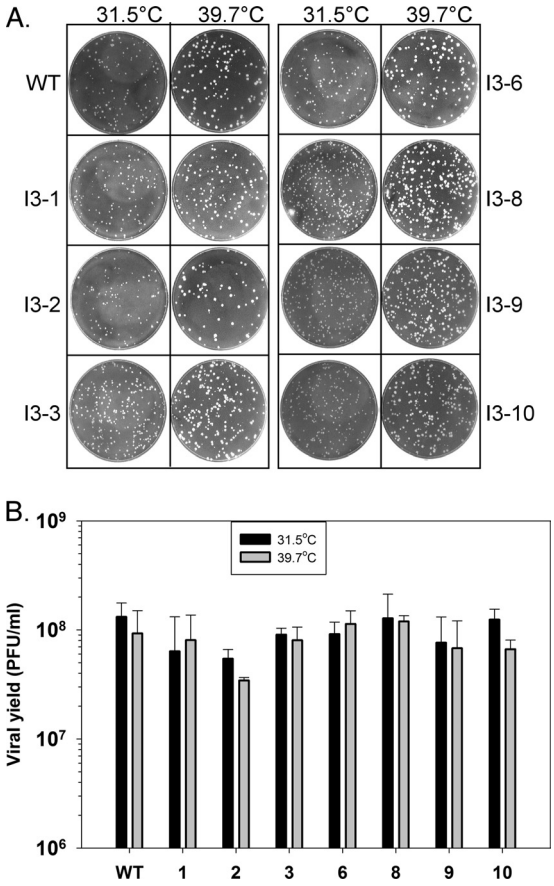

FIG 5 Analysis of I3 viral recombinants *in vivo*. Recombinant viruses were generated using transient dominant selection such that the endogenous I3 allele was replaced with one of the 10 clustered charge-to-alanine mutants described above. Viruses encoding seven of these alleles were readily purified. (A) Plaque assays were performed at both 31.5°C and 39.7°C (permissive and nonpermissive temperatures, respectively), and results were visualized by crystal violet staining after 48 h of infection. (B) At 24 h, viral yield was assessed utilizing these recombinant viruses at both permissive (black bars) and nonpermissive (gray bars) temperatures.

excess of what is needed to support DNA synthesis (10- to 12.5-fold reduction of I3 leads to an ~4-fold reduction in DNA accumulation) or that I3 plays a stimulatory but not essential role in DNA synthesis.

To gain further insight into how I3 depletion might affect DNA accumulation, we performed pulsed-field gel electrophoresis (PFGE) to assess the DNA species present at 8 and 12 hpi in cells treated with MM or si-I3 and then infected with WT virus (MOI of 3) (Fig. 6E). There was a clear diminution (~3- to 7-fold) in the levels of the mature, monomeric genome (~200 kb) (Fig. 6E, arrowhead) in cells treated with si-I3. We did not, however, see any evidence of unresolved concatemeric DNA, which would migrate more slowly than mature genomes, nor did we observe the reproducible accumulation of subgenomic species; in addition to the PFGE gel shown in Fig. 6, samples were analyzed under other electrophoretic conditions that allowed visualization of DNA as small as 200 bp (not shown).

Intracellular localization of I3: insight into the organization and structure of these factories. As shown in Fig. 6A and previously (42), I3 localizes to discrete foci within infected cells that are termed replication factories. The specificity of this localization is illustrated in Fig. 7A: whereas an I3-mCherry fusion protein localizes to discrete replication factories, the mCherry protein itself is dispersed throughout the cytoplasm. To test the hypothesis that the localization of I3 reflects its association with stable structures that might contain scaffolding proteins, cytoskeletal elements, or DNA-containing complexes, we assessed the retention or loss of I3 when cells were briefly prepermeabilized with Triton X-100 (0.1% for 30 s) prior to fixation for immunofluorescence analysis. Comparable protocols have been shown to release soluble proteins from the cytosol or nucleoplasm but not those anchored by association with the cytoskeleton or the nuclear matrix (4, 19, 28, 37). The diffuse pool of I3 (along with other cytosolic proteins) is lost during this prepermeabilization step, but the factory-associated I3 is anchored and is not diminished during prepermeabilization (Fig. 7B).

To obtain a higher resolution view of the $BrdU^+$, $I3^+$ replication factories shown in Fig. 6A, cells were harvested at 7 hpi (MOI of 2 in the presence of BrdU) for examination by conventional and immunoelectron microscopy. The most striking features seen were organelle-free zones within the cytoplasm (Fig. 7C) that were filled with material of even electron density (RF; replication factories) and appeared to be surrounded by double membranes (red arrowheads). Immunoelectron microscopy indicated that these delimiting membranes (Fig. 7D, red arrowheads) were labeled by an antibody to protein disulfide isomerase (PDI), a marker of the endoplasmic reticulum (ER) (Fig. 7D, red asterisks). The interior of the zones was labeled at high density with antibodies to BrdU (Fig. 7E, cyan asterisks), consistent with these zones being replication factories in which nascent DNA was being synthesized. These data reinforce the proposal (50, 56) that the replication of the poxvirus genome occurs within specialized, membrane-delimited cytoplasmic compartments.

DISCUSSION

The cytoplasmic localization of the poxviral life cycle necessitates that the virus encodes most, if not all, of its replication machinery. The poxvirus machinery must overcome the universal problems presented by the need to replicate a double-stranded DNA template, as well as solving the somewhat unique problems presented by replication within the cytoplasm, such as evading cytoplasmic DNA sensors (58). To compartmentalize replication and concentrate the precursors, enzymes, and template, poxviruses appear to induce the formation of membrane-delimited paddocks that are dedicated sites of replication (Fig. 7). These paddocks have been noted before and are referred to as "mininuclei" (50, 56). The I3 SSB described in the manuscript localizes to these sites of viral replication, which are the sites of accumulation of BrdU-labeled nascent DNA (Fig. 7). The paddocks appear to be delimited by PDI-positive (PDI^+) membranes derived from the ER, and it will be of interest in the future to understand how the ER membranes are recruited to enclose and shape these replication foci. Efficient replication in the cytoplasm may also provide the underlying rationale for why poxviruses encode such precursor-generating enzymes as ribonucleotide reductase (RR). An early report suggested that the viral ribonucleotide reductase interacted directly with the I3 protein (6), providing a mechanism whereby precursors might be synthesized at the site of utilization. Interestingly, it was the acidic C′ terminus of I3 that was shown to bind to the small subunit of the ribonucleotide reductase. Many SSBs have an acidic C

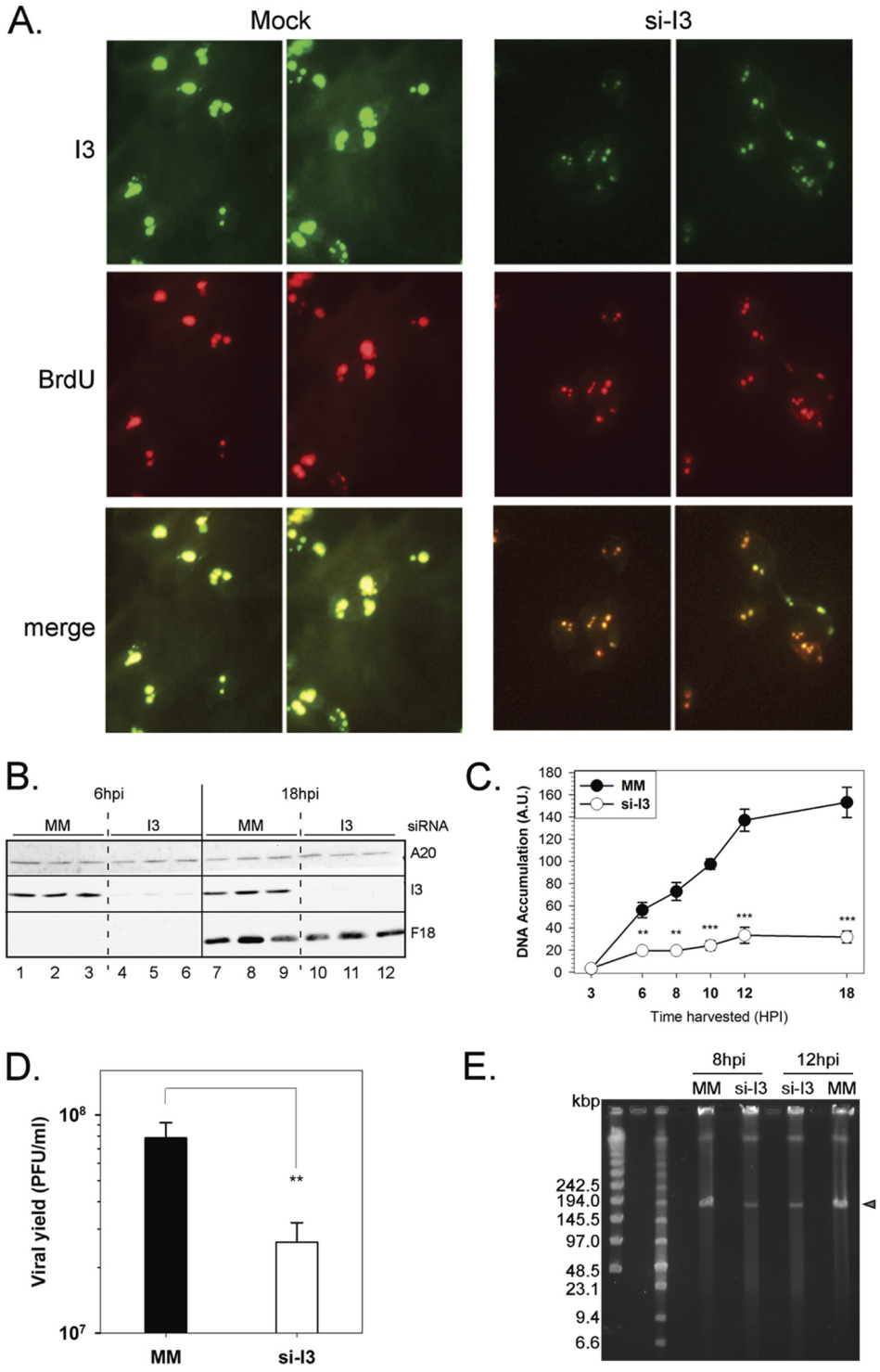

FIG 6 siRNA-mediated depletion of I3 during viral infection. (A) Immunofluorescence microscopy of nascent viral DNA depots. Infected cells were either mock treated or preloaded with I3-directed siRNA (si-I3) and fixed at 7 hpi for immunofluorescence microscopy. $I3^+$ and $BrdU^+$ foci colocalized, as visualized in the merge panels, and their relative sizes decreased in the presence of I3-specific siRNA. (B) Immunoblot analysis of siRNA-treated infected cells. Whole-cell lysates were probed for three viral proteins (A20, I3, and F18) to assess the specificity of the I3-directed siRNA. In triplicate, cells were preloaded with mismatch (MM) or I3 siRNA and harvested at 6 or 18 hpi for immunoblot analysis. (C) Southern dot blot analysis to measure viral DNA sequences. siRNA-treated cells were infected with WT virus, harvested at various times postinfection, and processed for Southern blot analysis. Viral sequences were detected using radiolabeled vaccinia virus sequences, quantitated, and plotted. Samples were spotted in quadruplicate, and bars represent standard deviations. **, $P < 0.02$; ***, $P < 0.001$. (D) Viral yield assessment. At 24 h viral yield was determined in WT-infected cells that had received either MM or I3-specific siRNA. **, $P < 0.02$. (E) Pulsed-field gel electrophoresis analysis of the nascent viral genomes after siRNA-directed I3 depletion. BSC40 cells were pretreated with siRNA (MM or si-I3) for 18 h prior to infection with WT virus (MOI of 3). At 8 and 12 hpi, cells were harvested and analyzed by PFGE as described in Materials and Methods section; the DNA was visualized by ethidium bromide staining. The arrowhead denotes the migration of full-length monomeric genomes.

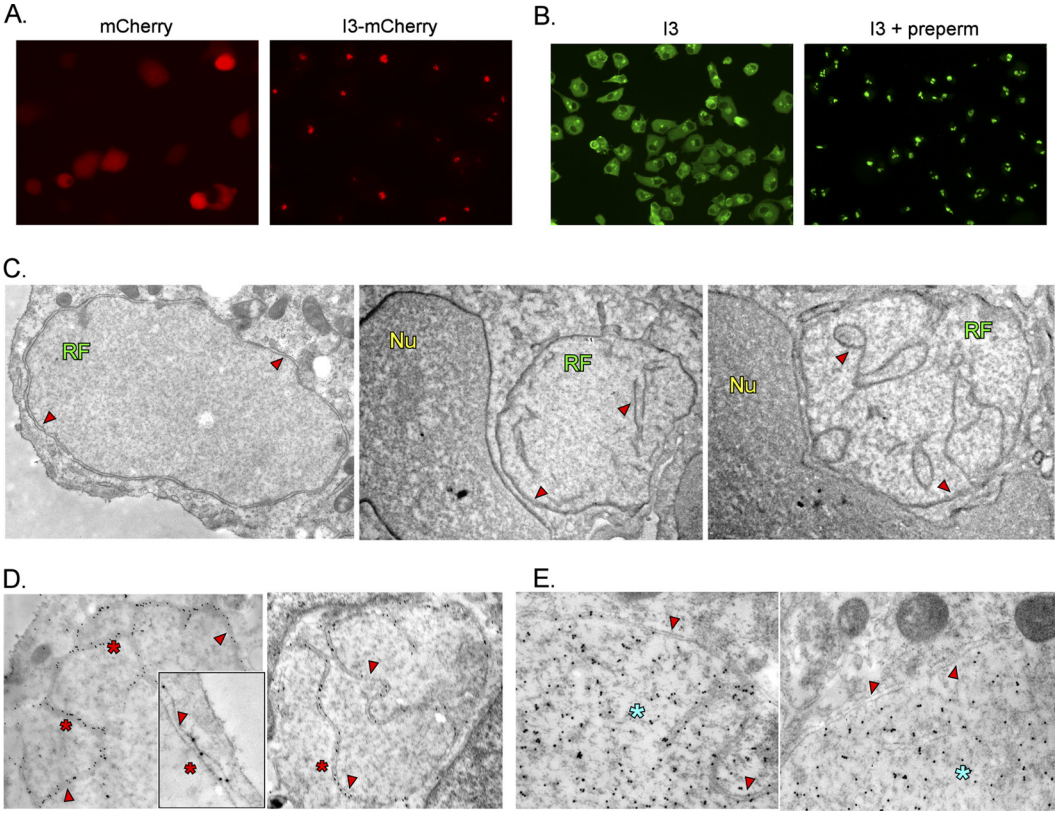

FIG 7 Visualization of replication factories by electron and immunofluorescence microscopy. (A) Fluorescence microscopic visualization of I3-mCherry in vaccinia virus-infected cells. Cells were infected with WT virus and transfected with plasmids encoding mCherry or I3-mCherry and visualized by fluorescence microscopy at 7 hpi (594 nm). (B) Immunofluorescence microscopy showing retention of I3 within replication factories. Cells were infected with WT virus for 7 h and then either prepermeabilized with 0.1% Triton X-100 for 30 s prior to fixation (right panel) or fixed directly (left panel). Both sample sets were then processed for immunofluorescence microscopy using the anti-I3 antibody. (C) Visualization of replication factories by electron microscopy. Cells were infected with WT virus for 7 h and then examined by electron microscopy. RF, replication factories; Nu, nucleus; red arrowheads, double membranes surrounding and penetrating the replication factories. (D and E) Immunoelectron microscopic examination of replication factories. Cells were infected with WT virus for 7 h in the presence of BrdU and then processed for immunoelectron microscopy. Sections were probed with anti-PDI (D) or anti-BrdU (E) antibodies and a 10 nm gold-labeled secondary antibody. Red arrowheads indicate double membranes that delimit the replication factories; red asterisks highlight their staining with the anti-PDI antibody. Cyan asterisks indicate the heavy labeling of the interior of the replication factories with the anti-BrdU antibody.

terminus, and this region has been shown to coordinate interactions with a plethora of core components of the replication apparatus as well as auxiliary proteins involved in diverse aspects of DNA metabolism (20, 31, 48). I3 has very recently been shown to bind to the cellular translation initiation factor eIF4G, which relocalizes to viral factories after infection (60). The possibility that the abundant I3 protein mediates the selective redistribution of a host translation factor is an intriguing observation and an area for future study.

Single-stranded DNA binding proteins (SSBs) are ubiquitous components of all replicative systems studied to date, and there is strong evidence that SSBs also play integral roles in DNA repair and DNA recombination. I3 fulfills the properties of an SSB by binding single-stranded DNA tightly and with great specificity (42, 53). Although the primary sequences of SSBs are quite diverse, the majority have been shown to contain one or more OB (oligonucleotide/oligosaccharide-binding) folds; this structural domain is comprised of a five-stranded beta sheet coiled to form a closed beta-barrel (36). We have utilized a variety of structural prediction programs, such as PHYRE (23), Swiss Model (1, 24), and i-Tasser (43, 44), to probe for conserved structural domains in the I3 protein, to no avail. These modeling algorithms failed to discern the presence of any OB folds or other conserved structural motifs within I3. Although structural prediction programs failed to identify an OB fold in the herpes simplex virus (HSV)-encoded SSB (ICP8), a region containing a similar set of ß-sheets and a motif of aromatic and basic residues was identified in the solved structure (30). The SSB from the bacterium *Thermoproteus tenax* (38) lacks an OB fold and binds DNA through a unique sequence that resides immediately upstream of a C-terminal multimerization domain. The DNA binding cleft of this SSB is also lined with phenylalanine residues and flanked by basic residues. The adenovirus SSB lacks an OB fold, and its binding is also mediated by a cleft containing key phenylalanine and basic residues (54). A conserved pattern and spacing of aromatic and basic residues were identified within the SSBs of *E. coli*, several bacteriophages, and several herpesviruses (55), and we have identified such a possible motif in the I3 protein (Fig. 1, blue circles). It will be of interest in the future to determine whether targeted mutagenesis of these residues impairs the interaction of I3 with DNA; if so, we would expect that such alleles would be unable to support virus viability. Of course, solution of the

crystal structure of I3 would greatly illuminate the mechanism by which it binds to ssDNA.

With the goal of gaining further insight into the contribution of I3 to the replication, recombination, and repair of the vaccinia virus genome, we utilized clustered charge-to-alanine mutagenesis to generate 10 mutant alleles of I3. Seven of these alleles were able to support virus viability *in vivo*, and the viruses encoding these alleles formed WT-sized plaques at both 31.5 and 39.7°C; moreover, no defect in 24-h viral yield was seen during single-cycle infections (Fig. 5). In contrast, we were unable to isolate viruses in which the endogenous I3 locus expressed I3-4, -5, or -7, despite repeated attempts. We believe that these alleles are unable to support viral replication.

To investigate the ability of the proteins encoded by the 10 targeted alleles to multimerize, the mutant proteins and WT I3 were expressed *in vitro* using IVTT. Each of the mutant proteins was able to interact with WT I3 *in vitro*, but the I3-4, -5, and -7 proteins were severely impaired in their ability to interact with themselves or with each other (Fig. 2). We also expressed and purified His_6-tagged forms of WT I3 and each of the 10 mutant proteins, and the multimerization defects of I3-4, -5, and -7 were confirmed by gel filtration analysis (Fig. 3). These data suggest that these amino acid substitutions, which span a 51-residue region of the protein, may perturb the I3-I3 interaction interface. Interestingly, these were the only three mutants that were unable to support virus viability *in vivo*. Additionally, as stated above, it has been previously proposed that the acidic C-terminal 81 amino acids (aa) of I3 can mediate an interaction with the small subunit of the viral ribonucleotide reductase (RR) (6). The lesions within the I3-5 and -7 alleles fall within this domain, and the subtle changes introduced in these I3 proteins may be sufficient to disrupt the I3-RR interaction and may contribute to their inability to support viral replication *in vivo*.

These purified preparations of His_6-I3 were also examined for DNA binding activity *in vitro* using EMSAs. The I3-6 protein showed a modest decrease in DNA binding activity (Fig. 4), but a virus encoding only I3-6 was not compromised *in vivo* (Fig. 5). *In vivo*, a high local concentration of I3 may be sufficient to overcome some reduction in intrinsic DNA binding activity. I3-5 was more severely impaired in its ability to bind to ssDNA, and, as mentioned above, it was unable to multimerize *in vitro* or to support viral replication *in vivo*. Although we have reported that the interaction of I3 with ssDNA *in vitro* is not cooperative (42), multimerization may play an important role *in vivo*. In fact, most SSBs are known to function as multimers, and often self-interaction juxtaposes the DNA-binding sites in a manner that stabilizes and enhances DNA binding (27, 39, 41). Thus, even though I3-4 and -7 can bind DNA oligonucleotides *in vitro* as assayed by EMSA, their DNA binding activities may not be optimal or sufficient *in vivo*.

Hence, while both DNA binding and the ability to form higher-order complexes appear to be important for the biological activity of I3 *in vivo*, we do not believe that they are intrinsically linked. Self-association of I3 was verified by yeast two-hybrid analysis (32; also data not shown), the interaction of 3×FLAG-I3 and His_6-I3 *in vitro* (Fig. 2), and gel filtration chromatography (Fig. 3). Our data confirm that I3 forms higher-order complexes, but the determination of the precise stoichiometry of these complexes and the impact of solution conditions and ssDNA on complex formation are areas for future study. In addition to enhancing I3-DNA interactions, multimerization of I3 may also present a novel binding surface for the recruitment of other viral proteins involved in replication, recombination, or repair.

We have previously reported that the I3 protein is phosphorylated during infection (42). Recombinant I3 and endogenous I3 exhibit comparable ssDNA binding properties (42, 53), signifying that phosphorylation is not required for the I3-DNA interaction. Moreover, the data presented here indicate that phosphorylation is also not required for I3-I3 multimerization. However, the identification of the sites on which I3 is phosphorylated and the subsequent determination of whether these modification events are important *in vivo* will shed further light on how I3 contributes to viral DNA metabolism.

By analogy to many other systems, it is reasonable to propose that I3 may play a significant role in DNA replication, recombination, and repair. A single-strand annealing (SSA) mechanism that relies on the 3′-5′ exonuclease activity of the viral polymerase has been proposed for the high levels of homologous recombination that occur during poxvirus infections (14). The I3 protein has been shown to stimulate polymerase-mediated strand-joining *in vitro* (59), and partial depletion of I3 (3- to 6.5-fold reduction) has been shown to halve the frequency of recombination *in vivo* (14) while reducing the levels of viral DNA replication by ~3-fold. Our siRNA protocol has enabled us to reduce the levels of I3 by 10- to 20-fold (Fig. 6B), which leads to a 4- to 7-fold reduction in DNA accumulation (Fig. 6C and E) and an ~3.5-fold reduction in infectious virus production (Fig. 6D). We were somewhat surprised that the impact of I3 depletion on viral DNA synthesis was not more drastic and postulate either that I3 is present in excess or that it plays a stimulatory, but not essential, role in viral DNA replication. The latter conclusion seems unlikely, given our earlier inability to isolate a virus in which the I3 locus has been deleted (42); generation of an I3-expressing cell line that might support the replication of a ΔI3 virus would be another possible approach to test the essentiality of I3. As a complement to the dot blot hybridization assay used to assess the levels of DNA synthesis (Fig. 6C) (14), PFGE analysis (Fig. 6E) verified that depletion of I3 caused a diminution in the levels of mature, monomeric genome that accumulated during infection. This diminution was not accompanied by a concomitant increase in unresolved genomes or subgenomic fragments. These data suggest that replication is slow and/or inefficient when I3 levels are low.

In sum, the cell biological, genetic, and biochemical data presented in this study expand our understanding of the vaccinia virus-encoded I3 single-stranded DNA-binding protein. The evaluation of 10 mutant alleles of I3 *in vitro* and *in vivo* and the assessment of siRNA-mediated depletion of I3 *in vivo* provided the first substantive genetic analysis of the contribution of I3 to viral replication. These data confirm that the ability of I3 to multimerize is associated with its ability to support viral replication *in vivo* and identify a region of the protein whose perturbation impairs multimerization. Further evaluation of the interaction of I3 with other proteins involved in DNA metabolism, a more thorough evaluation of the mechanism by which I3 interacts with ssDNA, and an assessment of how I3 is regulated by posttranslational modification will be areas of interest for future study.

ACKNOWLEDGMENTS

We thank Jill Lindgren for excellent technical support in the laboratory and Clive Wells for his superb assistance with electron microscopy. We

also thank Marilyn Khanna and Tyler Molitor for their input during the course of this project.

The work was supported by National Institutes of Health grant 2 R01 AI21858 (awarded to P.T.).

REFERENCES

1. **Arnold K, Bordoli L, Kopp J, Schwede T.** 2006. The SWISS-MODEL workspace: a web-based environment for protein structure homology modelling. Bioinformatics **22**:195–201.
2. **Boyle K, Traktman P.** 2009. Poxviruses, p 225–247. *In* Cameron CE, Gotte M, Raney KD (ed), Viral genome replication. Springer, New York, NY.
3. **Boyle KA, Arps L, Traktman P.** 2007. Biochemical and genetic analysis of the vaccinia virus d5 protein: multimerization-dependent ATPase activity is required to support viral DNA replication. J. Virol. **81**:844–859.
4. **Brown S, Levinson W, Spudich JA.** 1976. Cytoskeletal elements of chick embryo fibroblasts revealed by detergent extraction. J. Supramol. Struct. **5**:119–130.
5. **Cassetti MC, Merchlinsky M, Wolffe EJ, Weisberg AS, Moss B.** 1998. DNA packaging mutant: repression of the vaccinia virus A32 gene results in noninfectious, DNA-deficient, spherical, enveloped particles. J. Virol. **72**:5769–5780.
6. **Davis RE, Mathews CK.** 1993. Acidic C terminus of vaccinia virus DNA-binding protein interacts with ribonucleotide reductase. Proc. Natl. Acad. Sci. U. S. A. **90**:745–749.
7. **D'Costa SM, et al.** 2010. Vaccinia H5 is a multifunctional protein involved in viral DNA replication, postreplicative gene transcription, and virion morphogenesis. Virology **401**:49–60.
8. **DeMasi J, Traktman P.** 2000. Clustered charge-to-alanine mutagenesis of the vaccinia virus H5 gene: isolation of a dominant, temperature-sensitive mutant with a profound defect in morphogenesis. J. Virol. **74**:2393–2405.
9. **De Silva FS, Lewis W, Berglund P, Koonin EV, Moss B.** 2007. Poxvirus DNA primase. Proc. Natl. Acad. Sci. U. S. A. **104**:18724–18729.
10. **Evans E, Klemperer N, Ghosh R, Traktman P.** 1995. The vaccinia virus D5 protein, which is required for DNA replication, is a nucleic acid-independent nucleoside triphosphatase. J. Virol. **69**:5353–5361.
11. **Evans E, Traktman P.** 1987. Molecular genetic analysis of a vaccinia virus gene with an essential role in DNA replication. J. Virol. **61**:3152–3162.
12. **Evans E, Traktman P.** 1992. Characterization of vaccinia virus DNA replication mutants with lesions in the D5 gene. Chromosoma **102**:S72–S82.
13. **Falkner FG, Moss B.** 1990. Transient dominant selection of recombinant vaccinia viruses. J. Virol. **64**:3108–3111.
14. **Gammon DB, Evans DH.** 2009. The 3′-to-5′ exonuclease activity of vaccinia virus DNA polymerase is essential and plays a role in promoting virus genetic recombination. J. Virol. **83**:4236–4250.
15. **Garcia AD, Moss B.** 2001. Repression of vaccinia virus Holliday junction resolvase inhibits processing of viral DNA into unit-length genomes. J. Virol. **75**:6460–6471.
16. **Grubisha O, Traktman P.** 2003. Genetic analysis of the vaccinia virus I6 telomere-binding protein uncovers a key role in genome encapsidation. J. Virol. **77**:10929–10942.
17. **Hassett DE, Condit RC.** 1994. Targeted construction of temperature-sensitive mutations in vaccinia virus by replacing clustered charged residues with alanine. Proc. Natl. Acad. Sci. U. S. A. **91**:4554–4558.
18. **Hassett DE, Lewis JI, Xing X, DeLange L, Condit RC.** 1997. Analysis of a temperature-sensitive vaccinia virus mutant in the viral mRNA capping enzyme isolated by clustered charge-to-alanine mutagenesis and transient dominant selection. Virology **238**:391–409.
19. **He S, Sun JM, Li L, Davie JR.** 2005. Differential intranuclear organization of transcription factors Sp1 and Sp3. Mol. Biol. Cell **16**:4073–4083.
20. **He ZG, Rezende LF, Willcox S, Griffith JD, Richardson CC.** 2003. The carboxyl-terminal domain of bacteriophage T7 single-stranded DNA-binding protein modulates DNA binding and interaction with T7 DNA polymerase. J. Biol. Chem. **278**:29538–29545.
21. **Ishii K, Moss B.** 2001. Role of vaccinia virus A20R protein in DNA replication: construction and characterization of temperature-sensitive mutants. J. Virol. **75**:1656–1663.
22. **Kato SE, et al.** 2008. Marker rescue mapping of the combined Condit/Dales collection of temperature-sensitive vaccinia virus mutants. Virology **375**:213–222.
23. **Kelley LA, Sternberg MJ.** 2009. Protein structure prediction on the Web: a case study using the Phyre server. Nat. Protoc. **4**:363–371.
24. **Kiefer F, Arnold K, Kunzli M, Bordoli L, Schwede T.** 2009. The SWISS-MODEL Repository and associated resources. Nucleic Acids Res. **37**:D387–D392.
25. **Klemperer N, McDonald W, Boyle K, Unger B, Traktman P.** 2001. The A20R protein is a stoichiometric component of the processive form of vaccinia virus DNA polymerase. J. Virol. **75**:12298–12307.
26. **Klemperer N, Ward J, Evans E, Traktman P.** 1997. The vaccinia virus I1 protein is essential for the assembly of mature virions. J. Virol. **71**:9285–9294.
27. **Kur J, Olszewski M, Dlugolecka A, Filipkowski P.** 2005. Single-stranded DNA-binding proteins (SSBs)—sources and applications in molecular biology. Acta Biochim. Pol. **52**:569–574.
28. **Lenk R, Ransom L, Kaufmann Y, Penman S.** 1977. A cytoskeletal structure with associated polyribosomes obtained from HeLa cells. Cell **10**:67–78.
29. **Liu K, Lemon B, Traktman P.** 1995. The dual-specificity phosphatase encoded by vaccinia virus, VH1, is essential for viral transcription in vivo and in vitro. J. Virol. **69**:7823–7834.
30. **Mapelli M, Panjikar S, Tucker PA.** 2005. The crystal structure of the herpes simplex virus 1 ssDNA-binding protein suggests the structural basis for flexible, cooperative single-stranded DNA binding. J. Biol. Chem. **280**:2990–2997.
31. **Marintcheva B, Hamdan SM, Lee SJ, Richardson CC.** 2006. Essential residues in the C terminus of the bacteriophage T7 gene 2.5 single-stranded DNA-binding protein. J. Biol. Chem. **281**:25831–25840.
32. **McCraith S, Holtzman T, Moss B, Fields S.** 2000. Genome-wide analysis of vaccinia virus protein-protein interactions. Proc. Natl. Acad. Sci. U. S. A. **97**:4879–4884.
33. **McDonald WF, Traktman P.** 1994. Overexpression and purification of the vaccinia virus DNA polymerase. Protein Expr. Purif. **5**:409–421.
34. **Moss B, De Silva FS.** 2006. Poxvirus, p 707–727. *In* DePamphilis M (ed), DNA replication and human disease. Cold Spring Harbor Laboratory Press, Cold Spring Harbor, NY.
35. **Moyer RW, Graves RL.** 1981. The mechanism of cytoplasmic orthopoxvirus DNA replication. Cell **27**:391–401.
36. **Murzin AG.** 1993. OB(oligonucleotide/oligosaccharide binding)-fold: common structural and functional solution for non-homologous sequences. EMBO J. **12**:861–867.
37. **Pasdar M, Nelson WJ.** 1988. Kinetics of desmosome assembly in Madin-Darby canine kidney epithelial cells: temporal and spatial regulation of desmoplakin organization and stabilization upon cell-cell contact. II. Morphological analysis. J. Cell Biol. **106**:687–695.
38. **Paytubi S, et al.** 2012. Displacement of the canonical single-stranded DNA-binding protein in the *Thermoproteales*. Proc. Natl. Acad. Sci. U. S. A. **109**:E398–E405.
39. **Pestryakov PE, Lavrik OI.** 2008. Mechanisms of single-stranded DNA-binding protein functioning in cellular DNA metabolism. Biochemistry (Mosc.) **73**:1388–1404.
40. **Punjabi A, et al.** 2001. Clustered charge-to-alanine mutagenesis of the vaccinia virus A20 gene: temperature-sensitive mutants have a DNA-minus phenotype and are defective in the production of processive DNA polymerase activity. J. Virol. **75**:12308–12318.
41. **Richard DJ, Bolderson E, Khanna KK.** 2009. Multiple human single-stranded DNA binding proteins function in genome maintenance: structural, biochemical and functional analysis. Crit. Rev. Biochem. Mol. Biol. **44**:98–116.
42. **Rochester SC, Traktman P.** 1998. Characterization of the single-stranded DNA binding protein encoded by the vaccinia virus I3 gene. J. Virol. **72**:2917–2926.
43. **Roy A, Kucukural A, Zhang Y.** 2010. I-TASSER: a unified platform for automated protein structure and function prediction. Nat. Protoc. **5**:725–738.
44. **Roy A, Xu D, Poisson J, Zhang Y.** 2011. A protocol for computer-based protein structure and function prediction. J. Vis. Exp. **57**:e3259.
45. **Senkevich TG, Koonin EV, Moss B.** 2009. Predicted poxvirus FEN1-like nuclease required for homologous recombination, double-strand break repair and full-size genome formation. Proc. Natl. Acad. Sci. U. S. A. **106**:17921–17926.
46. **Shaner NC, et al.** 2004. Improved monomeric red, orange and yellow fluorescent proteins derived from *Discosoma* sp. red fluorescent protein. Nat. Biotechnol. **22**:1567–1572.
47. **Stanitsa ES, Arps L, Traktman P.** 2006. Vaccinia virus uracil DNA glycosylase interacts with the A20 protein to form a heterodimeric processivity factor for the viral DNA polymerase. J. Biol. Chem. **281**:3439–3451.

48. **Taylor TJ, Knipe DM.** 2004. Proteomics of herpes simplex virus replication compartments: association of cellular DNA replication, repair, recombination, and chromatin remodeling proteins with ICP8. J. Virol. **78**:5856–5866.
49. **Theobald DL, Mitton-Fry RM, Wuttke DS.** 2003. Nucleic acid recognition by OB-fold proteins. Annu. Rev. Biophys. Biomol. Struct. **32**:115–133.
50. **Tolonen N, Doglio L, Schleich S, Krijnse-Locker J.** 2001. Vaccinia virus DNA replication occurs in endoplasmic reticulum-enclosed cytoplasmic mini-nuclei. Mol. Biol. Cell **12**:2031–2046.
51. **Traktman P, Boyle K.** 2004. Methods for analysis of poxvirus DNA replication. Methods Mol. Biol. **269**:169–186.
52. **Traktman P, et al.** 2000. Elucidating the essential role of the A14 phosphoprotein in vaccinia virus morphogenesis: construction and characterization of a tetracycline-inducible recombinant. J. Virol. **74**:3682–3695.
53. **Tseng M, Palaniyar N, Zhang W, Evans DH.** 1999. DNA binding and aggregation properties of the vaccinia virus I3L gene product. J. Biol. Chem. **274**:21637–21644.
54. **Tucker PA, et al.** 1994. Crystal structure of the adenovirus DNA binding protein reveals a hook-on model for cooperative DNA binding. EMBO J. **13**:2994–3002.
55. **Wang YS, Hall JD.** 1990. Characterization of a major DNA-binding domain in the herpes simplex virus type 1 DNA-binding protein (ICP8). J. Virol. **64**:2082–2089.
56. **Welsch S, Doglio L, Schleich S, Krijnse LJ.** 2003. The vaccinia virus I3L gene product is localized to a complex endoplasmic reticulum-associated structure that contains the viral parental DNA. J. Virol. **77**:6014–6028.
57. **Wickramasekera NT, Traktman P.** 2010. Structure/function analysis of the vaccinia virus F18 phosphoprotein, an abundant core component required for virion maturation and infectivity. J. Virol. **84**:6846–6860.
58. **Wiebe MS, Traktman P.** 2007. Poxviral B1 kinase overcomes barrier to autointegration factor, a host defense against virus replication. Cell Host Microbe **1**:187–197.
59. **Willer DO, Yao XD, Mann MJ, Evans DH.** 2000. In vitro concatemer formation catalyzed by vaccinia virus DNA polymerase. Virology **278**:562–569.
60. **Zaborowska I, Kellner K, Henry M, Meleady P, Walsh D.** 2012. Recruitment of host translation initiation factor eIF4G by the Vaccinia Virus ssDNA-binding protein I3. Virology **425**:11–22.